Scientia Iranica C (2019) 26(3), 1516–1528

Sharif University of Technology
Scientia Iranica
Transactions C: Chemistry and Chemical Engineering
http://scientiairanica.sharif.edu

The application of non-Fourier and Fick's laws to the flow of temperature-dependent thermal conductivity generalized Newtonian liquids: A 3D computational study

M. Khan[a], L. Ahmad[a,b,*], W. Azeem Khan[a,c], and A. Saleh Zuhair Al Shamrani[d]

a. *Department of Mathematics, Quaid-i-Azam University, Islamabad 44000, Pakistan.*
b. *Department of Mathematics, Shaheed Benazir Bhutto University, Sheringal Upper Dir 18000, Pakistan.*
c. *Department of Mathematics and Statistics, Hazara University, Mansehra 21300, Pakistan.*
d. *Department of Mathematics, Faculty of Science, King Abdulaziz University, Jeddah 21589, Saudi Arabia.*

Received 2 December 2017; received in revised form 11 March 2018; accepted 10 December 2018

KEYWORDS
3D Sisko liquid;
Generalized heat flux and mass diffusion relations;
Temperature-dependent thermal conductivity.

Abstract. The current article presents a numerical study for local solutions of Sisko liquid flow by a bidirectional stretched surface. In addition, the analysis of relaxation times for the heat and mass transfer mechanisms is conducted by utilizing modified heat flux and mass diffusion models. These improved relations are the generalized form of Fourier and Fick's laws in which the time-space upper-convected derivative is employed to portray the heat conduction and mass diffusion mechanisms. Appropriate transformations lead to a strongly nonlinear differential system of equations that are then solved numerically by employing the applications of bvp4c package in Matlab software. Another numerical method, namely shooting technique, with RK45 Fehlberg and Newton-Raphson method is utilized to authenticate the results. Graphical illustrations demonstrating the impacts of sundry physical parameters with required discussion highlighting their physical effects are also a part of this exploration. It is perceived that the temperature and concentration of Sisko liquid are the diminishing functions of relaxation times for the heat and mass transfer mechanisms. It is also fascinating to note that the temperature and concentration of Sisko liquid are higher in the classical form than that in the improved constitutive relation.

1. Introduction

Heat conduction and mass diffusion are broad mechanisms in nature and have received great attention from researchers and engineers owing to their extensive range of applications in industrial and engineering projects such as cooling of nuclear reactors, heat conduction in tissues and electronic devices, power generation, etc. Characteristics of heat and mass transfer phenomena have been explored adequately based on the Fourier and Fick's laws for the heat conduction and mass diffusion, respectively, in recent years. Several researchers have presented a study on flow and heat and mass transfer. In this regard, Liao and Pop [1] analytically discussed similarity boundary layer equations explicitly. Alam and Ahammad [2] addressed the features of variable heat and mass transfer and fluxes over an inclined stretching sheet. Isaa et al. [3] considered exponential variations of bounded permeable shrinking sheet during the boundary layer flow of Casson fluid with magnetic and mixed

*. *Corresponding author.*
E-mail address: latifahmad@math.qau.edu.pk (L. Ahmad)

doi: 10.24200/sci.2018.5693.1425

convection effects. Ramly et al. [4] investigated the impacts of thermal radiation on the boundary layer flow over a radially stretching surface with zero and non-zero fluxes. Khan [5] examined a series solution of visco-elastic fluid flow over the shrinking/stretching surface with magnetic field effect. Furthermore, many researchers [6-8] focused their attention on such types of work to fill the gap.

However, the aforementioned studies suffer from a drawback, that is, these classical laws contradict the principle of causality and produce parabolic energy and concentration equations. The propagation speed of heat and mass disturbance is finite when introducing the thermal and concentration relaxation times in the Fourier and Fick's models. Cattaneo [9] revised the Fourier's law by using a relaxation time-dependent term in the energy equation to evade the paradox of heat conduction appliance. It is estimated that the addition of time-dependent relaxation to the energy equation converts the parabolic equation into a hyperbolic energy equation due to which heat energy is transported with limited speed in the form of propagation of thermal waves. Furthermore, these waves have numerous applications in areas such as nanofluids and skin burns. Christov [10] modified the Cattaneo relation that efficiently preserved the material-invariant formulation. Ciarletta and Straughan [11] demonstrated the uniqueness and stability of the modified heat conduction and mass diffusion relation. Hayat et al. [12] inspected the features of the developed heat conduction relation on an Oldroyd-B fluid by using chemical processes. They perceived from their observations that the temperature of Sisko liquid experiences falloff for boosted values of relaxation time parameter. Khan and Khan [13] analyzed the characteristics of 3D flow of Burgers liquid for the developed heat conduction relation. They detected from their observations that the temperature of the Burgers liquid extensively affected the augmented values of relaxation time parameter. Waqas et al. [14] investigated the characteristics of variable thermal conductivity and developed the heat conduction relation for generalized Burgers liquid. Sui et al. [15] studied the impact of developed double diffusion relations for the Maxwell nanofluid. The features of the developed heat conduction relation on magneto viscoelastic liquid over a stretched surface were explored by Liu et al. [16]. The effects of improved heat conduction and mass diffusion models on 3D Burgers fluid flow by utilizing chemical processes were investigated by Khan et al. [17]. Malik et al. [18] presented a numerical study of magneto-Casson fluid flow with variable viscosity and Cattaneo-Christove heat flux model. Muhammad et al. [19] scrutinized the features of Cattaneo-Christove heat and mass flux models in squeezing nanofluid flow. The characteristics of non-Fourier and Fick's laws respecting Jeffery nanofluid flow over an inclined stretching surface were illustrated by Khan et al. [20].

The massive utility of nonlinear materials has substantially involved scientists and engineers in their study during the past few decades. In particular, such nonlinear liquids are involved in paper production, oil reservoir engineering, geophysics, bioengineering, chemical and nuclear industries, polymer solution and cosmetic processes, etc. As a consequence, different types of non-linear relations have been suggested according to the features of nonlinear liquids. Amongst these nonlinear materials, Sisko liquid relation is considered to predict the shear thinning and shear thickening properties of fluids. Munir et al. [21] scrutinized the characteristics of convective flow with the heat conduction mechanism over a bidirectional stretching surface for Sisko liquid flow. Khan et al. [22] explored the features of the convectively heated surface for the Sisko liquid. Malik et al. [23] inspected the features of random motion and thermophoresis for the Sisko liquid flow. Khan et al. [24] studied the numerical analysis of improved heat conduction and mass diffusion models for flow of Sisko liquid. They concluded from their graphical observations that the temperature and concentration profiles were significantly affected by the power-law index when it intensified from $n < 1$ to $n > 1$. The numerical investigation of radiative magneto-Sisko nanofluid flow was reported by Khan et al. [25]. Furthermore, a large number of attempts were made to study such fluids flow, heat, and mass transfer phenomena; many of them are addressed in [26-28].

To study the impact of thermal relaxation parameters on 3D steady Sisko liquid flow, the Cattaneo-Christove model is utilized. Likewise, this fluid model is considered to incorporate the shear thinning ($0 < n < 1$) and shear thickening ($n > 1$) properties of fluids in the presence of generalized Fourier and Fick's laws. Fourier [29] suggested a well-known law of heat conduction, which is commonly used for heat conduction aspects when revealed up in the literature. Later on, this phenomenon has come to be commonly recognized as the paradox of heat conduction. Throughout the literature, no available study considers exploring the characteristics of thermal and concentration diffusions introduced by Cattaneo-Christov fluxes. However, the phenomena of heat and mass transfer arise when there exist temperature and concentration differences between the components of a similar body. These phenomena have massive technological and industrial use, e.g., in cooling of atomic reactors, microelectronics, pasteurization of food, fuel cells, power generation, energy production, etc. This impact on the fluid flow is responsible for the temperature balance in the flow of fluid. Every flow parameter with a significant influence is studied through the graphs of temperature and concentration. To model internal temperature

profiles, an accurate determination and distribution of heat source along with thermal conductivities of various components is required. Owing to the role of this source, the cooling system is maintained on the external side of the battery or external side of the battery pack. In addition, enhanced thermal management will promote the maturing conception of neighborhood instrument and may increase superior battery outlines and upgraded lifetimes. At last, considering interior temperature profiles at high current densities provides a chance to anticipate and stay away from conditions for thermal escape, which is a key well-being constraint for LIBs amid procedure at the existing high densities. The second important effect of this physical property has been utilized in this work for the first time in the flow of 3D steady Sisko liquid.

Regarding the aforesaid studies and their enormous applications, the intention of the current article is to intensely explore the impact of modified heat flux and mass diffusion models on 3D Sisko liquid flow. The problem under consideration is modeled in the form of a set of highly nonlinear Partial Differential Equations (PDEs), which are then transformed into coupled nonlinear Ordinary Differential Equations (ODEs) by utilizing appropriate transformations. The numerical results are achieved by utilizing the bvp4c function in Matlab. In addition, graphical illustrations that emphasize the effects of various prominent parameters with their physical importance are given.

2. Mathematical formulation

Let us consider the 3D flow of Sisko liquid in the region $z > 0$. The flow is induced by a bidirectional stretched surface with velocities $u = cx$ and $v = dy$, where c and d are taken as constants, as shown in Figure 1. The velocity, temperature, concentration, and stress fields are assumed to be dependent on x, y, and z. The features of relaxation times of heat conduction and mass diffusion are taken in the energy equation to visualize the impact of these time-dependent terms on the energy and concentration involving Sisko liquid. On the stretched surface, the temperature and concentration of Sisko liquid take the value (T_w, C_w), while the concentration of Sisko liquid far away from the stretched surface takes these values (T_∞, C_∞), respectively. Based on the overhead assumptions, the governing equations [15,24] for Sisko liquid flow can be expressed as follows:

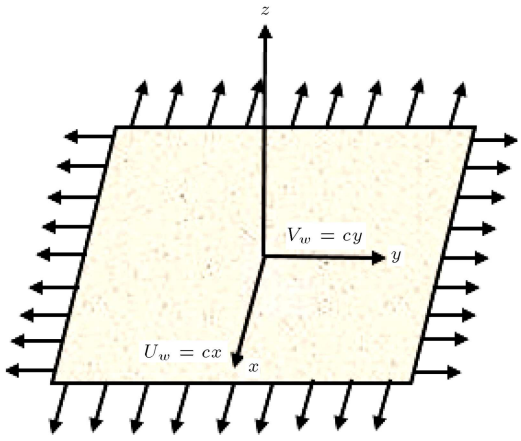

Figure 1. Flow geometry for the bidirectional stretching surface.

$$div\mathbf{V} = 0, \tag{1}$$

$$\rho_f \left(\mathbf{V}.\nabla\right)\mathbf{V} = -\nabla p + \nabla.\mathbf{S}, \tag{2}$$

$$\rho c_f \left(\mathbf{V}.\nabla\right)\mathbf{T} = \nabla.\mathbf{q}, \tag{3}$$

$$\left(\mathbf{V}.\nabla\right)\mathbf{C} = \nabla.\mathbf{J}, \tag{4}$$

where:

$$\mathbf{S} = \left[a + b\left|\sqrt{\frac{1}{2}tr\left(\mathbf{A}_1\right)^2}\right|^{n-1}\right]\mathbf{A}_1. \tag{5}$$

In Eq. (5), $A_1 = (grad\mathbf{V}) + (grad\mathbf{V})^T$ is the first Rivilin-Ericksen tensor. The general form of modified Fourier and Fick's laws is considered in [15], as written in the following:

$$\mathbf{q}+\delta_E\left(\frac{\partial\mathbf{q}}{\partial t} + \mathbf{V}\cdot\nabla\mathbf{q} - \mathbf{q}\cdot\nabla\mathbf{V} + (\nabla\cdot\mathbf{V})\mathbf{q}\right) = -k\left(T\right)\nabla T, \tag{6}$$

$$\mathbf{J}+\delta_C\left(\frac{\partial\mathbf{J}}{\partial t} + \mathbf{V}\cdot\nabla\mathbf{J} - \mathbf{J}\cdot\nabla\mathbf{V} + (\nabla\cdot\mathbf{V})\mathbf{J}\right) = -D\nabla C, \tag{7}$$

where $k\ (T)$ is the temperature-dependent thermal conductivity as follows:

$$k\left(T\right) = k_\infty\left(1 + \varepsilon\left(\frac{T - T_\infty}{T_w - T_\infty}\right)\right). \tag{8}$$

Eqs. (1) and (2) are reduced in the form of Eqs. (9) and (10). While energy and concentration conservation laws defined in Eqs. (3) and (4) take a form defined through Eqs. (12) and (13) (shown in Box I) by eliminating **q** from Eqs. (3) and (6) and **J** from Eqs. (4)

$$u\frac{\partial T}{\partial x}+v\frac{\partial T}{\partial y}+w\frac{\partial T}{\partial z}+\delta_E\left[\begin{array}{l} u^2\frac{\partial^2 T}{\partial x^2}+v^2\frac{\partial^2 T}{\partial y^2}+w\frac{\partial^2 T}{\partial z^2} \\ +2uv\frac{\partial^2 T}{\partial x\partial y}+2vw\frac{\partial^2 T}{\partial y\partial z}+2uv\frac{\partial^2 T}{\partial x\partial z} \\ +\left(u\frac{\partial u}{\partial x}+v\frac{\partial u}{\partial y}+w\frac{\partial u}{\partial z}\right)\frac{\partial T}{\partial x} \\ +\left(u\frac{\partial v}{\partial x}+v\frac{\partial v}{\partial y}+w\frac{\partial v}{\partial z}\right)\frac{\partial T}{\partial y} \\ +\left(u\frac{\partial w}{\partial x}+v\frac{\partial w}{\partial y}+w\frac{\partial w}{\partial z}\right)\frac{\partial T}{\partial z} \end{array}\right]=\frac{1}{(\rho c_p)_f}\frac{\partial}{\partial z}\left(k\left(T\right)\frac{\partial T}{\partial z}\right), \tag{12}$$

$$u\frac{\partial C}{\partial x}+v\frac{\partial C}{\partial y}+w\frac{\partial C}{\partial z}+\delta_C\left[\begin{array}{l} u^2\frac{\partial^2 C}{\partial x^2}+v^2\frac{\partial^2 C}{\partial y^2}+w\frac{\partial^2 C}{\partial z^2} \\ +2uv\frac{\partial^2 C}{\partial x\partial y}+2vw\frac{\partial^2 C}{\partial y\partial z}+2uv\frac{\partial^2 C}{\partial x\partial z} \\ +\left(u\frac{\partial u}{\partial x}+v\frac{\partial u}{\partial y}+w\frac{\partial u}{\partial z}\right)\frac{\partial C}{\partial x} \\ +\left(u\frac{\partial v}{\partial x}+v\frac{\partial v}{\partial y}+w\frac{\partial v}{\partial z}\right)\frac{\partial C}{\partial y} \\ +\left(u\frac{\partial w}{\partial x}+v\frac{\partial w}{\partial y}+w\frac{\partial w}{\partial z}\right)\frac{\partial C}{\partial z} \end{array}\right]=\frac{D}{(\rho c)_f}\frac{\partial^2 C}{\partial z^2}. \tag{13}$$

Box I

and (7) and will take the following form:

$$\frac{\partial u}{\partial x}+\frac{\partial v}{\partial y}+\frac{\partial w}{\partial z}=0, \tag{9}$$

$$u\frac{\partial u}{\partial x}+v\frac{\partial u}{\partial y}+w\frac{\partial u}{\partial z}=\frac{a}{\rho_f}\frac{\partial^2 u}{\partial z^2}-\frac{b}{\rho_f}\frac{\partial}{\partial z}\left(-\frac{\partial u}{\partial z}\right)^n, \tag{10}$$

$$u\frac{\partial v}{\partial x}+v\frac{\partial v}{\partial y}+w\frac{\partial w}{\partial z}=\frac{a}{\rho_f}\frac{\partial^2 v}{\partial z^2}+\frac{b}{\rho_f}\frac{\partial}{\partial z}\left(-\frac{\partial u}{\partial z}\right)^{n-1}\frac{\partial v}{\partial z}. \tag{11}$$

The corresponding boundary conditions are stated as follows:

$$u=U_w=cx,\quad v=V_w=dy,\quad w=0,\quad T=T_w,$$
$$\text{and}\quad C=C_w\quad \text{at } z=0, \tag{14}$$

$$u\to 0,\quad v\to 0,\quad T\to T_\infty,\quad C\to C_\infty$$
$$\text{as}\quad z\to\infty. \tag{15}$$

The final flow equations for such a fluid model are obtained while using suitable transformations as defined below:

$$u=cxf'\left(\eta\right),\quad v=cyg'(\eta),$$
$$w=-c\left(\frac{c^{n-2}}{\frac{\rho_f}{b}}\right)^{\frac{1}{n+1}}\left[\frac{2n}{n+1}f\left(\eta\right)+\frac{1-n}{1+n}\eta f'\left(\eta\right)+g(\eta)\right]x^{\frac{n-1}{n+1}}, \tag{4}$$

$$\theta\left(\eta\right)=\frac{T-T_\infty}{T_w-T_\infty},$$
$$\phi\left(\eta\right)=\frac{C-C_\infty}{C_w-C_\infty},$$
$$\eta=z\left(\frac{c^{2-n}}{\frac{b}{\rho_f}}\right)^{\frac{1}{n+1}}x^{\frac{1-n}{1+n}}. \tag{16}$$

By considering the transformations defined in Eq. (16), which identically satisfied Eq. (9) and Eqs. (10) to (13) along with the imposed boundary conditions defined through Eqs. (14) and (15), the dimensionless variable, η, can be obtained as follows:

$$Af'''+\left(\frac{2n}{n+1}\right)ff''+n\left(-f''\right)^{n-1}f'''+gf''-f'^2=0, \tag{17}$$

$$Ag'''+\left(\frac{2n}{n+1}\right)fg''+\left(-f''\right)^{n-1}g'''-g'^2-(n-1)g''f'''\left(-f''\right)^{n-2}+gg''=0, \tag{18}$$

$$\left(1+\varepsilon\theta\right)\theta''+\varepsilon\theta'^2+\Pr\left(\frac{2n}{n+1}\right)f\theta'+\Pr g\theta'-\Pr\lambda_E\left[\left(\frac{2n}{n+1}f+g\right)^2\theta''+\left(\frac{2n}{n+1}f'+g'\right)\left(\frac{2n}{n+1}f+g\right)\theta'\right]=0, \tag{19}$$

$$\phi'' - Sc\lambda_C\left[\left(\frac{2n}{n+1}f+g\right)^2\phi'' + \left(\frac{2n}{n+1}f'+g'\right)\left(\frac{2n}{n+1}f+g\right)\phi'\right] + Sc\left(\frac{2n}{n+1}\right)f\phi' + Scg\phi' = 0, \tag{20}$$

$$f(0)=0, \quad f'(0)=1, \; g(0)=0, \quad g'(0)=\alpha, \quad \theta(0)=1, \quad \phi(0)=1, \tag{21}$$

$$f'\to 0, \quad g'\to 0, \quad \theta\to 0, \quad \phi\to 0 \quad \text{as} \quad \eta\to\infty. \tag{22}$$

Here, all of the flow parameters are defined as follows:

Local Reynold numbers:

$$Re_a = \frac{U_w x\rho_f}{a}, \quad Re_b = \frac{U_w^{2-n}x^n\rho_f}{b},$$

Material parameterof Sisko liquid:

$$A = \frac{Re_b^{\frac{2}{n+1}}}{Re_a}.$$

Stretching ratio parameter:

$$\alpha = \frac{d}{c}.$$

Generalized Prandtl number:

$$\Pr = \frac{\rho c_p x U_w}{k_\infty} Re_b^{-\frac{2}{n+1}}.$$

Generalized Schmidt number:

$$Sc = \frac{xU_w Re_b^{-\frac{2}{n+1}}}{D}.$$

Relaxation parameters:

$$\lambda_E = \frac{U_w\delta_E}{x}, \quad \lambda_C = \frac{U_w\delta_C}{x}.$$

3. Physical quantities

Physical quantities involved in the flow problem have a special interest, as presented in this illustration. These physical quantities include the resistive forces and the rate of heat and mass transfer and can be expressed in the form of local skin friction, local Nusselt, and local Sherwood numbers. Moreover, the local Nusselt and Sherwood numbers can be obtained in the absence of relaxation parameters λ_E and λ_C. These are further defined as follows:

$$C_{fx} = \frac{\tau_{xz}}{\frac{1}{2}\rho U_w^2}, \quad C_{fy} = \frac{\tau_{yz}}{\frac{1}{2}\rho U_w^2}, \tag{23}$$

$$Nu_x = -\frac{x}{(T_f - T_\infty)}\left(\frac{\partial T}{\partial z}\right)\Big|_{z=0}, \tag{24}$$

$$3Sh_x = -\frac{x}{(C_w - C_\infty)}\left(\frac{\partial C}{\partial z}\right)\Big|_{z=0}. \tag{25}$$

The above expressions in dimensionless variables are given as follows:

$$\frac{1}{2}Re_b^{\frac{1}{n+1}}C_{fx} = Af''(0) - (-f''(0))^n, \tag{26}$$

$$\frac{1}{2}Re_b^{\frac{1}{n+1}}C_{fy} = \frac{V_w}{U_w}\left[Ag''(0) + (-f''(0))^{(n-1)}g''(0)\right], \tag{27}$$

$$Re^{-\frac{1}{n+1}}Nu_x = -\theta'(0), \tag{28}$$

$$Re^{-\frac{1}{n+1}}Sh_x = -\phi'(0). \tag{29}$$

4. Numerical scheme

The approach used for finding the computational results of the problem is one of the well-known collocation techniques known as bvp4c. If the computational results obtained during each iteration process are close to the exact results, then such a perception of closeness is stated as numerical stability. This closeness of the approximations results from the use of symmetric points at each subinterval of the whole interval. Moreover, a single solution rather than dual solutions generated by this technique will always be a more stable solution by keeping the step size smaller at the interval.

The transformed problem through Eqs. (17) to (20) along with the boundary conditions (21) and (22) is first converted into first-order ODEs by using some new variables. In this work, the tolerance level is fixed up to 10^{-6}. The main procedures of the aforementioned method are as follows:

$$f = x_1, \quad f' = x_2, \quad f'' = x_3, \quad f''' = x_3', \tag{30}$$

$$g = x_4, \quad g' = x_5, \quad g'' = x_6, \quad g''' = x_6', \tag{31}$$

$$\theta = x_7, \quad \theta' = x_8, \quad \theta'' = x_8', \tag{32}$$

$$\phi = x_9, \quad \phi' = x_{10}, \quad \phi'' = x_{10}', \tag{33}$$

then:

$$x_3' = \frac{-\left(\frac{2n}{1+n}\right)x_1x_3 + x_2^2 - x_4x_3}{A + n(-x_3)^{n-1}}, \tag{34}$$

$$x_6' = \frac{\left[(n-1)\,x_3'\,(-x_3)^{n-2} - \left(\frac{2n}{1+n}\right)x_1 - x_4\right]x_6 + x_5^2}{A + (-x_3)^{n-1}}, \tag{35}$$

$$x_8' = \frac{\varepsilon x_8^2 - \Pr\left[\left(\frac{2n}{1+n}\right)x_1 + x_4\right]x_8 + \Pr\lambda_E\left[\left\{\left(\frac{2n}{1+n}\right)x_1 + x_4\right\}\left\{\left(\frac{2n}{1+n}\right)x_2 + x_5\right\}x_8\right]}{1 + \varepsilon x_7 - \Pr\lambda_E\left\{\left(\frac{2n}{1+n}\right)x_1 + x_4\right\}^2}, \tag{36}$$

$$x_{10}' = \frac{Sc\lambda_C\left[\left\{\left(\frac{2n}{1+n}\right)x_1 + x_4\right\}\left\{\left(\frac{2n}{1+n}\right)x_2 + x_5\right\}x_{10}\right] + Sc\left[\left(\frac{2n}{1+n}\right)x_1 + x_4\right]x_{10}}{1 - Sc\lambda_C\left\{\left(\frac{2n}{1+n}\right)x_1 + x_4\right\}^2}. \tag{37}$$

Box II

Eqs. (35)-(37) are shown in Box II. Then, with the associated boundary conditions:

$$x_0(1) = 0, \quad x_0(2) = 1, \quad x_\infty(2) = 0, \tag{38}$$

$$x_0(4) = 0, \quad x_0(5) = \alpha, \quad x_\infty(5) = 0, \tag{39}$$

$$x_0(7) = 1, \quad x_0(9) = 1, \tag{40}$$

$$x_\infty(7) = 0, \quad x_\infty(9) = 0. \tag{41}$$

5. Testing of code

The graphical outcomes, as shown in Figures 2(a), (b) and 3(a), (b), that are obtained during the implementation of two different techniques, namely bvp4c package and shooting technique, with RK45 Fehlberg and Newton-Raphson method are in excellent agreement. In the absence of thermal relaxation times parameter, the resistive forces and the rate of heat and mass transfer are calculated by means of

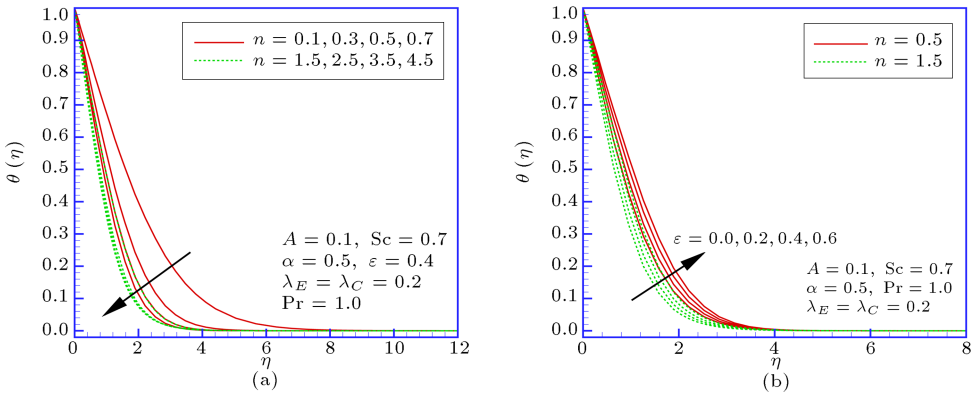

Figure 2. Comparison between bvp4c and shooting method.

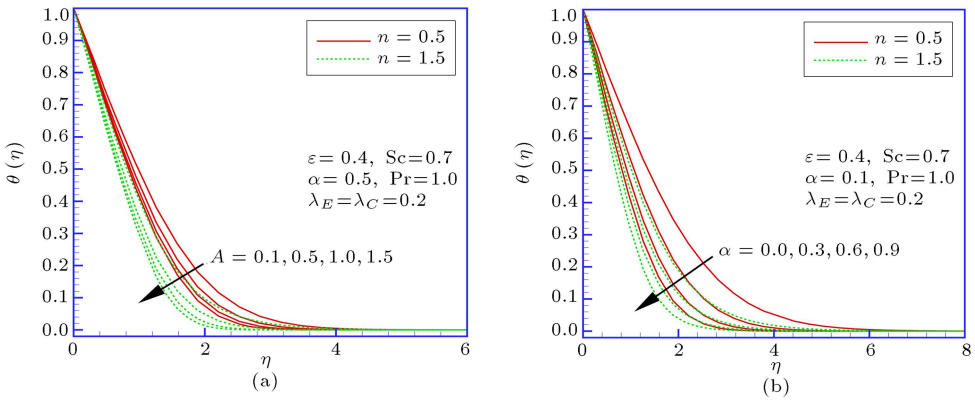

Figure 3. Comparison between bvp4c and shooting method.

Table 1. A comparison of different values of parameters α and A when $\lambda_E = \lambda_C = 0$, $\varepsilon = 0.2$, Pr = 1.0, and $Sc = 0.7$.

		$-\frac{1}{2}\mathrm{Re}_b^{\frac{1}{n+1}} C_{fx}$ $n = 0.5$		$-\frac{1}{2}\mathrm{Re}_b^{\frac{1}{n+1}} C_{fx}$ $n = 1.5$	
A	α	bvp4c results	Shooting results	bvp4c results	Shooting results
0.0	0.5	1.13996	1.13996	1.080836	1.081467
0.3		1.319315	1.319315	1.219016	1.219016
0.6		1.466857	1.466857	1.347461	1.347461
0.9		1.595912	1.595912	1.467824	1.467826
0.3	0.2	1.272579	1.27258	1.150458	1.150458
	0.4	1.304217	1.304217	1.196803	1.196803
	0.6	1.334019	1.33402	1.240703	1.240703
	0.8	1.362413	1.362413	1.282728	1.282728

Table 2. A comparison of different values of parameters α and A when $\lambda_E = \lambda_C = 0$, $\varepsilon = 0.2$, Pr = 1.0, and Sc = 0.7.

		$-\frac{1}{2}\mathrm{Re}_b^{\frac{1}{n+1}} C_{fy}\left(\frac{U_w}{V_w}\right)$ $n = 0.5$		$-\frac{1}{2}\mathrm{Re}_b^{\frac{1}{n+1}} C_{fy}\left(\frac{U_w}{V_w}\right)$ $n = 1.5$	
A	α	bvp4c results	Shooting results	bvp4c results	Shooting results
0.0	0.5	0.4880151	0.4880155	0.4631148	0.4631760
0.3		0.5612967	0.5612971	0.5226291	0.5226290
0.6		0.6219364	0.6219369	0.5781403	0.5781402
0.9		0.6580686	0.6580693	0.6301397	0.6301409
0.3	0.2	0.1808517	0.1808520	0.1683653	0.1683653
	0.4	0.4227907	0.4227911	0.3926630	0.3926630
	0.6	0.7098639	0.7098643	0.6633788	0.6633786
	0.8	1.0338740	1.0338740	0.9748519	0.9748517

Table 3. A comparison of different values of parameters α, A, ε, Pr, and Sc when $\lambda_E = \lambda_C = 0$.

				$-\mathrm{Re}_b^{-\frac{1}{n+1}} \mathrm{Nu}_x$ $n = 0.5$		$-\mathrm{Re}_b^{-\frac{1}{n+1}} \mathrm{Nu}_x$ $n = 1.5$	
α	A	ε	Pr	bvp4c results	Shooting results	bvp4c results	Shooting results
0.2	0.3	0.2	1.0	0.5027945	0.5027942	0.6291291	0.6291288
0.4				0.5629547	0.5629544	0.6791365	0.6791362
0.6				0.6149866	0.6149863	0.7244819	0.7244812
0.5	0.2	0.2	1.0	0.5821947	0.5821945	0.6925467	0.6925461
	0.4			0.5964440	0.5964438	0.7109888	0.7109881
	0.6			0.6077180	0.6077177	0.7258383	0.7258395
0.5	0.3	0.0	1.0	0.6743011	0.6743008	0.8055851	0.8055847
		0.2		0.5897737	0.5897734	0.7022954	0.7022948
		0.4		0.5272804	0.5272802	0.6256381	0.6256379
0.5	0.3	0.2	1.0	0.5897737	0.5897734	0.7022954	0.7022948
			1.2	0.6606327	0.6606324	0.7929611	0.7929601
			1.4	0.7261042	0.7261038	0.8762091	0.8762076

bvp4c, shooting technique, and the Homotopy Analysis Method (HAM), as shown in Tables 1 to 6. The results are found to be in excellent correlation. Furthermore, the tabular values, as shown in Table 7, are of high confidence that can validate the present work in the form of the rate of heat conduction with the result reported by [21].

6. Results and discussion

The focus of the current research work is to inspect the features of the developed heat conduction and mass diffusion relations for Sisko liquid over a bidirectional stretched surface. In this research work, the Matlab package bvp4c is implemented to find the numerical

Table 4. A comparison of different values of parameters α, A, and Sc when $\lambda_E = \lambda_C = 0$, $\varepsilon = 0.2$, and Pr=1.0.

			$-\mathbf{Re}_b^{-\frac{1}{n+1}}\mathbf{Sh}_x$ $n = 0.5$		$-\mathbf{Re}_b^{-\frac{1}{n+1}}\mathbf{Sh}_x$ $n = 1.5$	
α	A	Sc	bvp4c results	Shooting results	bvp4c results	Shooting results
0.2	0.3	0.7	0.4586049	0.4586047	0.5640612	0.5640610
0.4			0.5136857	0.5136855	0.6096096	0.6096094
0.6			0.5610952	0.5610950	0.6508408	0.6508405
	0.3	0.7	0.5381442	0.5381440	0.6306739	0.6306736
	0.6		0.5560509	0.5560507	0.6564534	0.6564526
	0.9		0.5695241	0.5695238	0.6759027	0.6759031
0.2	0.3	0.5	0.4318077	0.4318076	0.4935355	0.4935353
		0.7	0.5381442	0.5381440	0.6306739	0.6306736
		0.9	0.6313370	0.6313368	0.7505632	0.7505627

Table 5. A comparison of different values of parameter α when $\lambda_E = \lambda_C = 0$, $A = 0.2$, $\varepsilon = 0.2$, Pr = 1.0, and Sc = 0.7.

	$-\frac{1}{2}\mathbf{Re}_b^{\frac{1}{n+1}}\boldsymbol{C_{fx}}$ $n = 1$		$-\frac{1}{2}\mathbf{Re}_b^{\frac{1}{n+1}}\boldsymbol{C_{fy}}\left(\frac{U_w}{V_w}\right)$ $n = 1$	
α	bvp4c results	HAM results	bvp4c results	HAM results
0.2	1.138711	1.1387099	0.1629324	0.16293310
0.4	1.178466	1.1784669	0.3825393	0.38253890
0.6	1.215886	1.2158860	0.6468921	0.64689201
0.8	1.251533	1.2515337	0.9494035	0.94940360

Table 6. A comparison of different values of parameters ε and Sc when $\lambda_E = \lambda_C = 0$, $A = 0.2$, $\alpha = 0.5$, and Pr = 1.0.

	$-\mathbf{Re}_b^{-\frac{1}{n+1}}\mathbf{Nu}_x$ $n = 1$			$-\mathbf{Re}_b^{-\frac{1}{n+1}}\mathbf{Sh}_x$ $n = 1$	
ε	bvp4c results	HAM results	Sc	bvp4c results	HAM results
0.0	0.7569521	0.75694510	0.8	0.6531602	0.65315552
0.2	0.6606232	0.66061711	1.0	0.7569521	0.75694440
0.4	0.5892427	0.58928410	1.2	0.8509975	0.85105154
0.6	0.5338282	0.53382249	1.4	0.9375449	0.93773120

Table 7. A comparison of the present work and the published data for different values of α when $\lambda_E = \lambda_C = \mathrm{Sc} = \varepsilon = 0$, $A = 1.5$, and Pr = 1.0.

	$-\mathbf{Re}_b^{-\frac{1}{n+1}}\mathbf{Nu}_x$ $n = 0.5$		$-\mathbf{Re}_b^{-\frac{1}{n+1}}\mathbf{Nu}_x$ $n = 1.5$	
α	Present results	Munir et al. [21]	Present results	Munir et al. [21]
0.2	0.6218029	0.62074	0.7892013	0.78919
0.4	0.6956284	0.69468	0.8486394	0.84864
0.6	0.7604169	0.75957	0.9028750	0.90287
0.8	0.8190204	0.81827	0.9532423	0.95324

solution of the problem. Furthermore, the prime emphasis of the following debate is to investigate the impact of the governing physical parameters on the heat and mass transfer mechanisms for the Sisko liquid. Such parameters include power-law index (n), material parameter (A), stretching ratio parameter (α), variable thermal conductivity (ε), Prandtl number (Pr), thermal and concentration relaxation time parameters (λ_E, λ_C), and Schmidt number (Sc).

7. Temperature profile

7.1. Effect of n and ε on temperature profiles

Figure 4(a) and (b) represents the impacts of n and ε on the temperature profile of Sisko liquid flow. Based on these plots, one may recognize that the temperature of Sisko liquid decreases for the two cases, i.e., pseudoplastic as well as dilatant fluids with the increasing values of n. Significant results are obtained

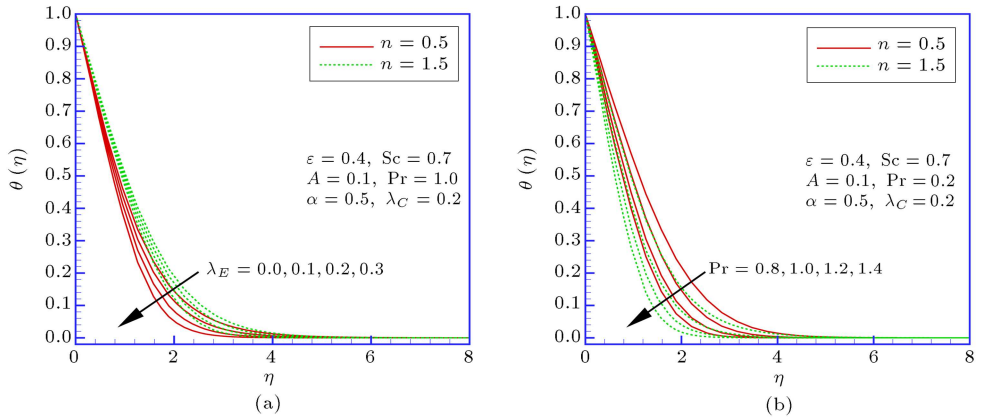

Figure 4. Impact of the power-law index and thermal conductivity parameter on temperature $\theta(\eta)$.

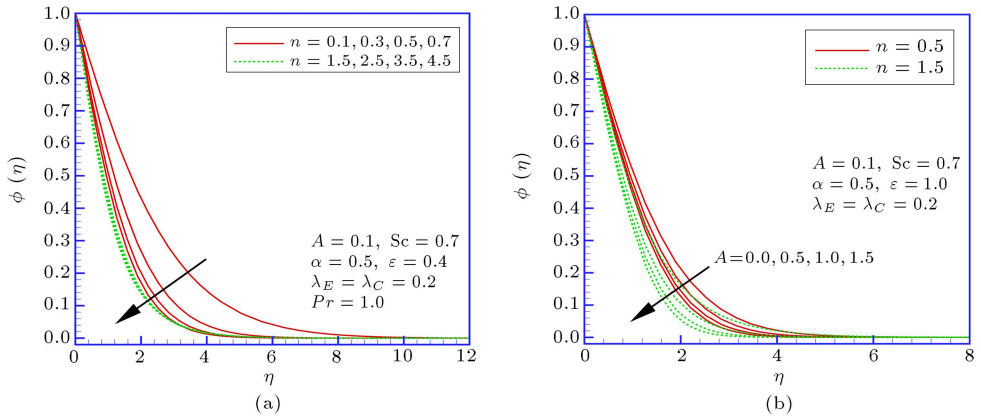

Figure 5. Impact of the material parameter and stretching ratio parameter on temperature $\theta(\eta)$.

with respect to pseudo-plastic liquid ($0 < n < 1$) as compared to dilatant ($n > 1$) liquid. Then, the temperature profile of the Sisko liquid is enhanced with the raising values of variable thermal conductivity. The numerical value $\varepsilon = 0$ shows that the Sisko liquid has constant conductivity. Besides, a low temperature is detected for the constant thermal conductivity and a higher temperature for variable thermal conductivity. Escalation of ε enhances the temperature profile of the liquid along with the thermal boundary layer thickness.

7.2. Effect of A and α on temperature profiles

The impact of material parameter A on the temperature profile is shown in Figure 5(a) and (b). Based on these figures it is presumed that the temperature of the liquid is declining with associated thermal boundary layer thickness, while using the growing values of A and α. The power-law index in this plot is considered based on the conditions of pseudoplastic ($0 < n < 1$) and dilatant ($n > 1$) liquids. From a physical perspective, the diminishing impact of the temperature of the liquid results from higher shear rate that produces low viscosity and, also, from the low shear rate that produces high viscosity with the rising values of A. Another variation in parameter α demonstrates a critical physical outcome. In other words, at any point, as the stretching on the surface builds up, the separation between the liquid particles expands, which is the reason why the temperature of the liquid abatements and the thickness of the thermal boundary layer are additionally decreasing.

7.3. Effect of λ_E and Pr on temperature profiles

Figure 6(a) and (b) exhibit the effect of the thermal relaxation parameter, λ_E, and Prandtl number Pr on the temperature profile. Based on these representations, an increase in λ_E prompts a decrease in the temperature profile and the thickness of the related thermal boundary layer. Physically, this is the direct result of the way that fluid particles require more opportunities for the exchange of heat to the closest adjoining particles of the liquid. The increase of λ_E demonstrates a non-conductor property of the liquid that causes a decrease in the temperature profile. The growing values of Pr cause a decrease while the temperature profile and related thermal boundary layer thickness are also reduced. Physically, this is the direct result of the

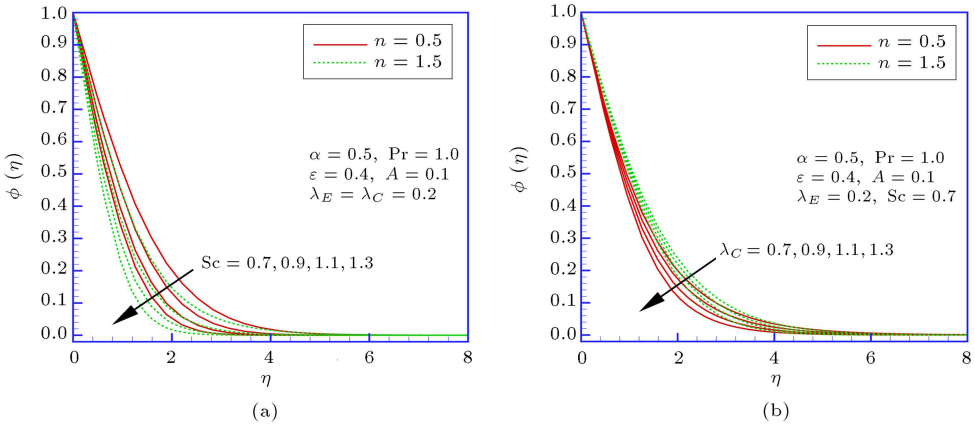

Figure 6. Impact of the relaxation time parameter and Prandtl number on temperature $\theta(\eta)$.

modified rate of heat dissemination with the raising values of Pr. For the higher values of Prandtl number, the diffusivity of liquid appears small; as a result, a reduction in the temperature field curves is depicted.

8. Concentration profile

8.1. *Effect of n and A on concentration profiles*

The vacillation resulting from n and A in concentration profile and the related boundary layer thickness is shown in Figure 7(a) and (b). According to these graphs, the concentration profile and related concentration boundary layer thickness are reduced as the values of n increase. An extremely significant outcome is observed during the variations in power-law index n between 0 and 1. In this plot, a reducing behavior in the dimensionless concentration profile and related boundary layer thickness for the particular values of A is illustrated. From a physical viewpoint, this is the direct result of the low share rate with higher viscosity of the liquid; accordingly, the low rate of mass diffusion is observed.

8.2. *Effect of Sc and λ_C on concentration profiles*

Various higher values of Sc and λ_C on concentration profile are shown in Figure 8(a) and (b). A decreasing behavior of the concentration profile and related concentration boundary layer thickness is seen because of the rising values of Sc and λ_C. The aforementioned figures are plotted while keeping n denoted by the physical properties of power-law liquids, i.e., pseudoplastic and dilatant liquids. Physically, an immediate connection between Sc and molecular diffusivity is found; at whatever point, the values of Sc are uplifted and an increase in the molecular diffusivity of the liquid arises and, accordingly, the concentration profile decreases.

9. Concluding remarks

In the present exploration, the characteristics of the boundary layer flow of 3D Sisko liquid over a bidirectional stretched surface were scrutinized. Additionally, the impacts of Cattaneo-Christov heat and mass flux models were also considered here. The numerical

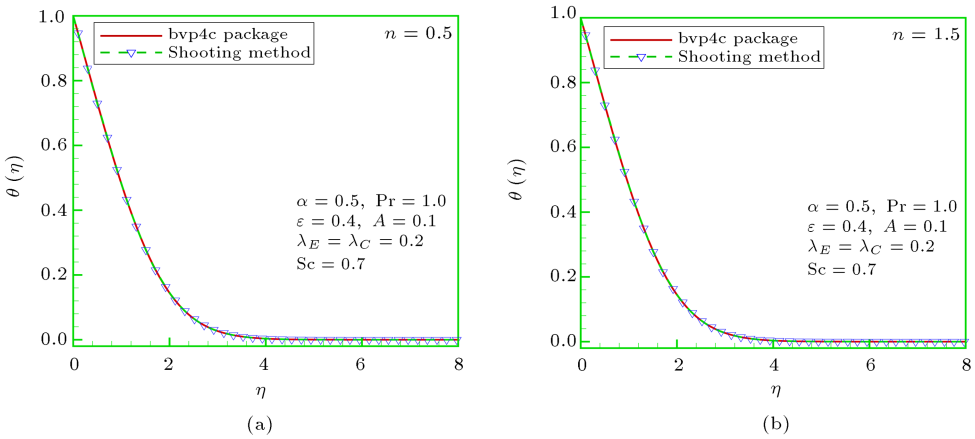

Figure 7. Impact of the power-law index and material parameter on concentration $\phi(\eta)$.

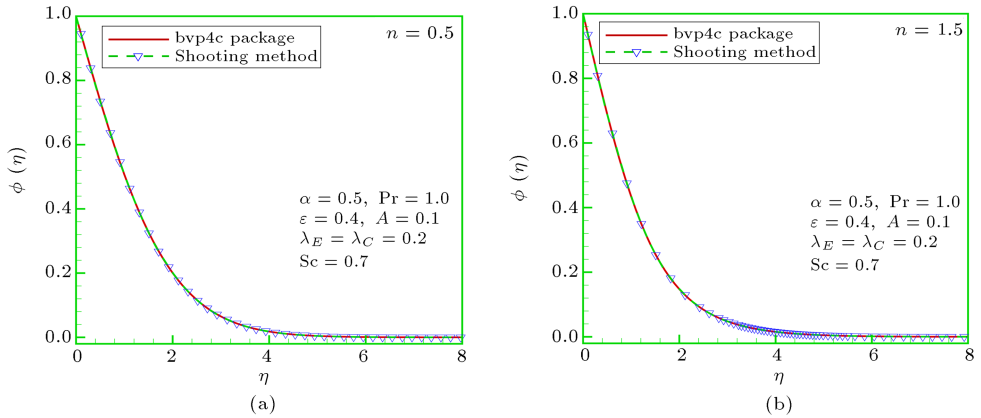

Figure 8. Impact of the Schmidt number and relaxation parameter on concentration $\phi(\eta)$.

technique, namely Matlab function bvp4c, was used to solve the modeled problem. Moreover, another computational method, namely shooting technique, was implemented to obtain the results. Interesting insights regarding the influence of various physical parameters that govern the problem were extracted. Significant findings of the problem are presented as follows:

- The power-law index caused a reduction in the temperature distribution;
- The temperature distribution declined with the larger value of thermal relaxation time;
- Temperature distribution was the declining function of the generalized Prandtl number;
- It was anticipated that the concentration profile diminished with the increase of the concentration relaxation time;
- A significant growing effect was noticed during the increasing values of variable thermal conductivity while plotting temperature profile.

Acknowledgements

The authors acknowledge the technical and financial support provided by the Deanship of Scientific Research (DSR) at Kin Abdulaziz University, Jeddah, Saudi Arabia. The authors would also like to thank the referee for valuable comments that enhanced the quality of the paper.

Nomenclature

u, v, w	Velocity components
a, b, n	Physical quantities of Sisko liquid
x, y, z	Cartesian coordinate system
$\mathbf{U}_w$, $\mathbf{V}_w$	Stretching velocities
$\mathbf{S}$	Extra stress tensor
∇	Nabla
$\mathbf{V}$	Velocity field
p	Fluid Pressure
T, C	Temperature and concentration of fluid
ρ_f, c_f	Fluid density and specific heat
α_1	Thermal diffusivity
D	Diffusion coefficient
T_∞ , C_∞	Ambient temperature and concentration of fluid
c_p	Specific heat at constant pressure
f, g	Dimensionless stream functions
$(\rho c)_f$	Heat capacity of base fluid
θ, ϕ	Dimensionless temperature and concentration
η	Dimensionless variable
ε	Thermal conductivity of fluid
k_∞	Thermal conductivity of fluid at infinite distance
ν	Kinematic viscosity
c	Constant
$\mathbf{q}, \mathbf{J}$	Normal heat and mass fluxes
t	Time
δ_E, δ_C	Relaxation times of heat and mass fluxes

References

1. Liao, S.J. and Pop, I. "Explicit analytic solution for similarity boundary layer equations", *Int. J. Heat Mass Transf.*, **47**(1), pp. 75-85 (2004).
2. Alam, M.S. and Ahammad, M.U. "Effects of variable chemical reaction and variable electric conductivity on free convective heat and mass transfer flow along an inclined stretching sheet with variable heat and mass fluxes under the influence of Dufour and Soret effects", *Nonlinear Anal. Model. Control*, **16**, pp. 1–16 (2011).

3. Isaa, S.S.P.M., Arifin, N.M., Nazarc, R., Bachok, N., Ali, F.M., and Pop, I. "MHD mixed convection boundary layer flow of a Casson fluid bounded by permeable shrinking sheet with exponential variation", *Scientia Iranica B*, **24**(2), pp. 637-647 (2017).
4. Ramly, N.A., Sivasankaran, S., and Noor, N.F.M. "Zero and nonzero normal fluxes of thermal radiative boundary layer flow of nano fluid over a radially stretched surface", *Scientia Iranica B*, **24**(6), pp. 2895-2903 (2017).
5. Khan, Y. "Magnetohydrodynamic flow of linear viscoelastic fluid model above a shrinking/stretching sheet: A series solution", *Scientia Iranica B*, **24**(5), pp. 2466-2472 (2017).
6. Niranjan, H., Sivasankaran, S., and Bhuvaneswari, M. "Chemical reaction, Soret and Dufour effects on MHD mixed convection stagnation point ow with radiation and slip condition", *Scientia Iranica B*, **24**(2), pp. 698-706 (2017).
7. Hussain, Q., Asghar, S., and Alsaedi, A. "Heat transfer analysis in peristaltic slip flow with Hall and ion-slip currents", *Scientia Iranica C*, **23**(6), pp. 2771-2783 (2016).
8. Heydari, M.M. "Investigation of fluid flow and heat transfer of compressible flow in a constricted microchannel", *Scientia Iranica B*, **23**(5), pp. 2144-2153 (2016).
9. Cattaneo, C. "Sulla conduzione Del Calore", *Atti Semin. Mat. Fis. Univ. Modena Reggio Emilia*, **3**, pp. 83-101 (1948).
10. Christov, C.I. "On frame indifferent formulation of the Maxwell-Cattaneo model of finite speed heat conduction", *Mech. Res. Commun.*, **36**, pp. 481-486 (2009).
11. Ciarletta, M. and Straughan, B. "Uniqueness and structural stability for the Cattaneo-Christov equations", *Mech. Res. Commun.*, **37**, pp. 445-447 (2010).
12. Hayat, T., Imtiaz, M., Alsaedi, A., and Almezal, S. "On Cattaneo-Christov heat flux in MHD flow of Oldroyd-B fluid with homogeneous-heterogeneous reactions", *J. Mol. Liq.*, **401**, pp. 296-303 (2016).
13. Khan, M. and Khan, W.A. "Three-dimensional flow and heat transfer to Burgers fluid using Cattaneo-Christov heat flux model", *J. Mol. Liq.*, **221**,pp. 651-657 (2016).
14. Waqas, M., Hayat, T., Farooq, M., Shehzad, S.A., and Alsaedi, A. "Cattaneo-Christov heat flux model for flow of variable thermal conductivity generalized Burgers fluid", *J. Mol. Liq.*, **220**, pp. 642-648 (2016).
15. Sui, J., Zheng, L., and Zhang, X. "Boundary layer heat and mass transfer with Cattaneo-Christov double-diffusion in upper-convected Maxwell nanofluid past a stretching sheet with slip velocity", *Int. J. Therm. Sci.*, **104**, pp. 461-468 (2016).
16. Liu, L., Zheng, L., Liu, F., and Zhang, X. "Anomalous convection diffusion and wave coupling transport of cells on comb frame with fractional Cattaneo-Christov flux", *Commun. Nonlinear Sci. Numer. Simulat.*, **38**, pp. 45-58 (2016).
17. Khan, W.A., Khan, M., and Alshomrani, A.S. "Impact of chemical processes on 3D Burgers fluid utilizing Cattaneo-Christov double-diffusion: Applications of non-Fourier's heat and non-Fick's mass flux models", *J. Mol. Liq.*, **223**, pp. 1039-1047 (2016).
18. Malik, M.Y., Khan, M., Salahuddin, T., and Khan, I. "Variable viscosity and MHD flow in Casson fluid with Cattaneo-Christov heat flux model: Using Keller box method", *Engi. Sci. Tech., Int. J.*, **19**(4), pp. 1985-1992 (2016).
19. Muhammad, N., Nadeem, S., and Mustafa, T. "Squeezed flow of a nanofluid with Cattaneo-Christov heat and mass fluxes", *Res. Phys.*, **7**, pp. 862-869 (2017).
20. Khan, M., Shahid, A., Malik, M.Y., and Salahuddin, T. "Thermal and concentration diffusion in Jeffery nanofluid flow over an inclined stretching sheet: A generalized Fourier's and Fick's perspective", *J. Mol. Liq.*, **251**, pp. 7-14 (2018).
21. Munir, A., Shahzad, A., and Khan, M. "Convective flow of Sisko fluid over a bidirectional stretching surface", *PLOS ONE*, **10**(6), e0130342 (2015).
22. Khan, M., Malik, R., Munir, A., and Khan, W.A. "Flow and heat transfer to Sisko nanofluid over a nonlinear stretching sheet", *PLOS ONE*, **10**(5), e0125683 (2015).
23. Malik, R., Khan, M., Munir, A., and Khan, W.A. "Flow and heat transfer in Sisko fluid with convective boundary condition", *PLOS ONE*, **9**(10), e107989 (2014).
24. Khan, W.A., Khan, M., Alshomrani, A.S., and Ahmad, L. "Numerical investigation of generalized Fourier's and Fick's laws for Sisko fluid flow", *J. Mol. Liq.*, **224**, pp. 1016-1021 (2016).
25. Khan, M., Ahmad, L., and Khan, W.A. "Numerically framing the impact of radiation on magnetonanoparticles for 3D Sisko fluid flow", *J. Braz. Soc. Mech. Sci. Eng.*, **39**(11), pp. 4475-4487 (2017).
26. Awais, M., Malik, M.Y., Bilal, S., Salahuddin, T., and Hussain, A. "Magnetohydrodynamic (MHD) flow of Sisko fluid near the axisymmetric stagnation point towards a stretching cylinder", *Res. Phys.*, **7**, pp. 49-56 (2017).
27. Hussain, A., Malik, M.Y., Salahuddin, T., Bilal, S., and Awais, M. "Combined effects of viscous dissipation and Joule heating on MHD Sisko nanofluid over a stretching cylinder", *J. Mol. Liq.*, **231**, pp. 341-352 (2017).
28. Hussain, A., Malik, M.Y., Bilal, S., Awais, M., and Salahuddin, T. "Computational analysis of magnetohydrodynamic Sisko fluid flow over a stretching cylinder in the presence of viscous dissipation and temperature dependent thermal conductivity", *Res. Phys.*, **7**, pp. 139-146 (2017).
29. Fourier, J.B.J., *Théorie Analytique De La Chaleur*, Paris (1822).

Biographies

Masood Khan was born in 1973 in Haripur, Khyber Pakhtunkhwa, Pakistan, He is currently a Professor at the Department of Mathematics, Quaid-i-Azam University, Islamabad, Pakistan. He received his BSc and MSc degrees in 1993 and 1997, respectively, from University of Peshawar, Khyber Pakhtunkhwa, Pakistan. He received his PhD degree in 2004 in Applied Mathematics, from Quaid-i-Azam University, Islamabad, Pakistan. His subject of interest is fluid mechanics as a researcher and a teacher.

Latif Ahmad was born in 1984 in Upper Dir, Khyber Pakhtunkhwa. He received his BS (Hons) degree in 2008 from University of Malakand at Chackdara, Khyber Pakhtunkhwa, Pakistan. He is Gold Medalist in BS. He received his MPhil degree in 2014 from University of Peshawar, Khyber Pakhtunkhwa, Pakistan in Applied Mathematics. He is also a permanent faculty member at the Department of Mathematics Shaheed Benazir Bhutto University, Sheringal Upper Dir, Khyber Pakhtunkhwa, Pakistan. He is on study leave for his PhD studies at the Department of Mathematics, Quaid-i-Azam University, Islamabad, Pakistan. His research interests include mathematical modeling and numerical simulation of Newtonian and non-Newtonian fluids flow. He has published thirteen papers in ISI Journals.

Waqar Azeem Khan was born in 1985 in Karachi, Pakistan. He received his MPhil degree in 2012 from Department of Mathematics, Quaid-i-Azam University, Islmabad, Pakistan. He is also a faculty member at Department of Mathematics and Statistics at Hazara University, Mansehra, Pakistan. He received his PhD degree in 2017 from Department of Mathematics, Quaid-i-Azam University, Islmabad, Pakistan. His research interests includes mathematical modeling and numerical simulation of non-Newtonian fluids flow. He has published forty papers in ISI Journals.

Ali Saleh Zuhair Al Shamrani was born in 1982 in the city of Baha, Saudi Arabia. He is currently a Professor at the Department of Mathematics, Faculty of Science, King Abdul Aziz University, Jeddah Saudi Arabia. His research interests are in the general areas of numerical analysis. He has also an excellent grade with second honor G. He remains a teacher for three years in the Ministry of Education, Saudi Arabia.